Runoff Variability in the Truckee–Carson River Basin from Tree Rings and a Water Balance Model

DAVID M. MEKO,[a] FRANCO BIONDI,[b] ALAN H. TAYLOR,[c] IRINA P. PANYUSHKINA,[a] RICHARD D. THAXTON,[a,d] ALEXANDER A. PRUSEVICH,[e] ALEXANDER I. SHIKLOMANOV,[e] RICHARD B. LAMMERS,[e] AND STANLEY GLIDDEN[e]

[a] *Laboratory of Tree-Ring Research, The University of Arizona, Tucson, Arizona*
[b] *DendroLab, Department of Natural Resources and Environmental Science, University of Nevada, Reno, Nevada*
[c] *Department of Geography and Earth and Environmental Systems Institute, The Pennsylvania State University, University Park, Pennsylvania*
[d] *Department of Earth and Spatial Sciences, University of Idaho, Moscow, Idaho*
[e] *Water Systems Analysis Group, Earth Systems Research Center, University of New Hampshire, Durham, New Hampshire*

(Manuscript received 24 October 2023, in final form 3 April 2024, accepted 18 April 2024)

ABSTRACT: Regional warming and associated changes in hydrologic systems pose challenges to water supply management in river basins of the western United States and call for improved understanding of the spatial and temporal variability of runoff. We apply a network of total width, subannual width, and delta blue intensity tree-ring chronologies in combination with a monthly water balance model to identify droughts and their associated precipitation P and temperature T footprints in the Truckee–Carson River basin (TCRB). Stepwise regression gave reasonably accurate reconstructions, from 1688 to 1999, of seasonal P and T (e.g., $R^2 = 0.50$ for May–September T). These were disaggregated to monthly values, which were then routed through a water balance model to generate "indirectly" reconstructed runoff. Reconstructed and observed annual runoff correlate highly ($r = 0.80$) from 1906 to 1999. The extended runoff record shows that twentieth-century droughts are unmatched in severity in a 300-yr context. Our water balance modeling reconstruction advances the conventional regression-based dendrochronological methods as it allows for multiple hydrologic components (evapotranspiration, snowmelt, etc.) to be evaluated. We found that imposed warming (3° and 6°C) generally exacerbated the runoff deficits in past droughts but that impact could be lessened and sometimes even reversed in some years by compensating factors, including changes in snow regime. Our results underscore the value of combining multiproxy tree-ring data with water balance modeling to place past hydrologic droughts in the context of climate change.

SIGNIFICANCE STATEMENT: We show how water balance modeling in combination with tree-ring data helps place modern droughts in the context of the past few centuries and a warming climate. Seasonal precipitation and temperature were reconstructed from multiproxy tree-ring data for a mountainous location near Lake Tahoe, and these reconstructions were routed through a water balance model to get a record of monthly runoff, snowmelt, and other water balance variables from 1688 to 1999. The resulting extended annual runoff record highlights the unmatched severity of twentieth-century droughts. A warming of 3°C imposed on reconstructed temperature generally exacerbates the runoff anomalies in past droughts, but this effect is sometimes offset by warming-related changes in the snow regime.

KEYWORDS: Paleoclimate; Tree rings; Regression analysis; Hydrologic models; Climate variability; Interannual variability

1. Introduction

Instrumental records over the past century have shown that the seasonal discharge regime of rivers and streams in the western United States varies substantially from year to year in response to the varied impact of large-scale ocean and atmospheric climate oscillations (Cayan et al. 1999; McCabe et al. 2008, 2004). At the same time, climate model simulations based on greenhouse warming show that moisture stress in the western United States is likely to increase (Garfin et al. 2013; Seager et al. 2007), with possibly drastic transformations of ecosystems and landscapes in the next decades as a consequence of severe heat waves and their effects on forests (Allen et al. 2010; Millar and Stephenson 2015; Trumbore et al. 2015). Properly evaluating modern changes and the likelihood of future changes benefits from a historical perspective that goes beyond the instrumental record to capture underlying long-term dynamics that would otherwise be impossible to detect (National Research Council 2006). The short instrumental record cannot fully capture the extent of hydroclimatic episodes lasting several decades that have affected the Sierra Nevada (e.g., Kleppe et al. 2011) and sometimes impacted widely separate major river basins of the western United

Supplemental information related to this paper is available at the Journals Online website: https://doi.org/10.1175/EI-D-23-0018.s1.

Corresponding author: David M. Meko, dmeko@arizona.edu

Earth Interactions is published jointly by the American Meteorological Society, the American Geophysical Union, and the Association of American Geographers.

DOI: 10.1175/EI-D-23-0018.1 e230018

States simultaneously (MacDonald et al. 2008; Meko et al. 2012).

Record extension is used in water resource management to improve estimates of average, extremes, and overall probability distributions of hydroclimatic parameters (Salas et al. 2016). Proxy records derived from growth layers of long-lived tree species have been used to augment time series of streamflow (Meko et al. 2001), precipitation (Gray et al. 2004), soil moisture (Yin et al. 2008), snow water equivalent (Woodhouse 2003), Palmer drought severity index (PDSI) (Cook et al. 2004), standardized precipitation index (Touchan et al. 2005), flood events (St. George and Nielsen 2003), and lake levels (Bégin 2001).

Streamflow, or discharge, reconstructions have long been applied in water resource studies to place the variability of the instrumental period in a multicentury context (Meko and Woodhouse 2011). They have also been applied for a context on general circulation model (GCM) projections of future droughts (Gray and McCabe 2010; Lutz et al. 2012), to identify ocean–atmosphere drivers of droughts and wet periods (Brito-Castillo et al. 2003; Hu et al. 2023) and to help decipher the causes of the rise and fall of ancient empires (Chen et al. 2022). Streamflow reconstructions are generally produced by statistical regression of a single hydrological parameter, such as water-year-total river discharge, on tree-ring chronologies or some linear combination of chronologies. The more advanced statistical models allow for special treatment of persistence and quantification of the uncertainty of reconstruction (Meko and Woodhouse 2011; Salas et al. 2015).

Reconstructing river discharge directly by regression of an observed discharge series on tree rings has clearly not only produced many useful reconstructions but also must be ultimately recognized as a "black box" approach. A reconstructed low annual discharge, for example, could be associated with very dry and cool conditions or alternatively with moderately dry and hot conditions. Statistics-only retrospective studies also ignore possible changes in the watershed (e.g., vegetative cover, channel morphology, and seasonality of climate) that change the relationship between moisture sensed by the trees and runoff reaching the gauge (Biondi and Strachan 2012). A promising new approach makes use of mechanistic watershed models (Gray and McCabe 2010; Lutz et al. 2012; Shamir et al. 2020), which offer the flexibility to incorporate assumptions on environmental conditions, to obtain spatially explicit reconstructions, and to test the sensitivity of reconstructed discharge to past watershed changes.

Such models have been recently applied in dendrohydrology at annual (Saito et al. 2008), seasonal (Solander et al. 2010), and monthly (Gray and McCabe 2010) time scales and can produce reconstructions of multiple components of the water balance, including streamflow, actual evapotranspiration, and snow water equivalent (Saito et al. 2015). The ability to model snowmelt and its relationship to temperature is critical in the western United States, where snowmelt can contribute as much as from 1/2 to 3/4 of the total annual runoff (Williams and Tarboton 1999) and where the snowmelt contribution is likely to be altered under climate change scenarios (Klos et al. 2014; Wieder et al. 2022). Climatological water balance (WB) models that operate on a monthly time scale and require only precipitation and temperature as time series input are especially suitable for hydrologic reconstruction because the climate inputs can be derived from tree rings using regression-based approaches. Widely used in dendrohydrology is the McCabe–Wolock monthly water balance model (McCabe and Wolock 2007; McCabe and Markstrom 2007), which has been applied for interpretation of dendrohydrologic signals in North America (Gray and McCabe 2010; Gangopadhyay et al. 2015) and North Africa (Meko et al. 2020).

In this paper, we apply the McCabe–Wolock WB model to the tree-ring reconstruction of runoff in the Truckee–Carson River basin (TCRB), at the boundary between Nevada and California in the western United Sates. The TCRB was chosen because of the societal importance of water supply in connection with the Lake Tahoe basin, the Reno/Sparks urban centers, the rural and native American communities in those basins, and the multiple ecological services that depend on TCRB freshwater. In addition, besides the availability of key data, including hydrologic, climatic, and tree-ring records, these basins have been the target of recent reconstructions of natural flows by conventional methods (Biondi and Meko 2019; Harris and Csank 2023). We contrast two ways of reconstructing annual runoff through a WB model. In the direct approach, the observed WB model output runoff summed over the water year is regressed on tree-ring data in the reconstruction model. What we broadly refer to as indirect reconstruction of runoff is regression-based reconstruction of annual or seasonal climate variables from tree-rings, followed by routing of those reconstructions—after temporal disaggregation, if needed—through a WB model (e.g., Saito et al. 2008; Gray and McCabe 2010; Meko et al. 2020). Indirect reconstruction is more complicated than direct reconstruction but gives the possibility of examining separate impacts of precipitation P and temperature T on runoff variations. Briefly, the steps in our implementation of indirect reconstruction are as follows: 1) seasonal total P and seasonal average T climate variables are regressed on tree-ring data to get reconstructed P and T; 2) the seasonal climate reconstructions are statistically disaggregated to monthly values, which are routed through the WB model to get monthly output runoff (and other water balance variables); and 3) WB model output is summed over months to get the indirectly reconstructed annual runoff.

A challenge to indirect reconstruction is capturing seasonal P and T signals with tree rings. To this end, our newly developed tree-ring network includes chronologies of total width, subannual width (Griffin et al. 2011), and delta blue intensity (Babst et al. 2016; Reid and Wilson 2020; Heeter et al. 2021; Yue et al. 2023). Instead of attempting to reconstruct full-basin runoff, we focus on "point" runoff, or the output of the WB model at a specified latitude, longitude, and elevation. The point might be a key location for contribution to basin runoff, or be important for some other diagnostic reason (e.g., coordinates of a tree-ring site). We apply the WB model to a set of selected points at a wide range of elevations and assess whether the model runoff from one or more points effectively summarizes the interannual variability of basin runoff as measured by natural flows from records at stream gauges. One

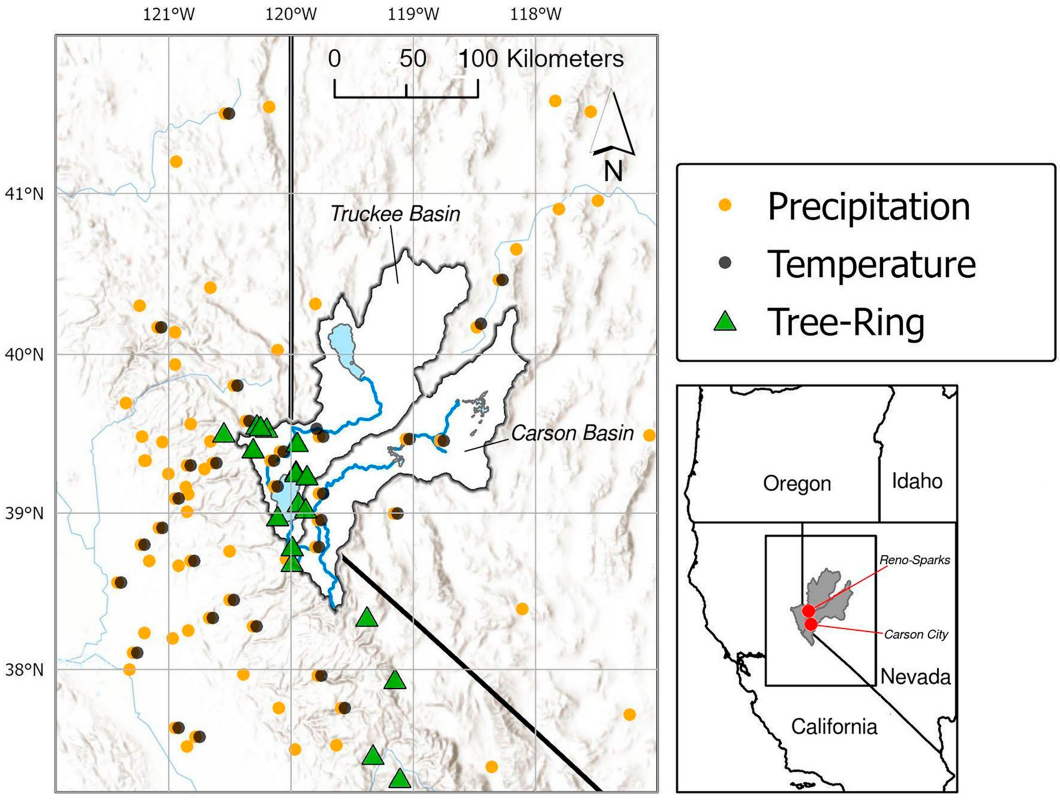

FIG. 1. Truckee–Carson Basin and locations of climatic stations and tree-ring chronologies. Climate network includes 73 GHCN precipitation and 32 temperature stations. Tree-ring network comprises 31 chronologies, but there are fewer points because of multiple species or data types at some coordinates. The basin includes three of Nevada's largest cities (inset map), including Reno, with an estimated population exceeding 273 000 in 2022 (U.S. Census Bureau 2024).

objective of this paper is to evaluate whether a multivariable tree-ring network can effectively reconstruct the seasonal precipitation P and temperature T needed as WB model input for indirect reconstruction of runoff. A second objective is to determine whether the runoff history, especially the record of drought severity, differs appreciably depending on whether generated by direct or indirect reconstruction. Finally, we seek to illustrate how tree-ring data combined with WB modeling can be used for clues to the sensitivity of runoff during past droughts in the TCRB to changing temperature and watershed conditions.

2. Data and methods

a. Study area

The TCRB is the combined basin of the Truckee (7900 km^2) and Carson (10 000 km^2) Rivers, which drain northeastward from the Sierra Nevada near Lake Tahoe (Fig. 1). Elevation ranges from more than 3000 m in the Sierra Nevada to less than 1200 m at the terminus of the Truckee River at Pyramid Lake and of the Carson River in the Carson Sink. The TCRB includes the cities of Reno and Sparks, Nevada, as well as numerous smaller cities and the highly developed recreation area around Lake Tahoe. Water issues are a major concern in the TCRB. More than 400 000 people depend on the flow of the two rivers, with competing demands from municipalities, agriculture, industry, and recreation (Bureau of Reclamation 2015, 2021). Steep climatic gradients related to elevation characterize the basin. Mean annual precipitation ranges from more than 180 cm in the high Sierra to less than 13 cm in the Carson Sink and is about 81 cm at Tahoe City, at an elevation of 1908 m on the shore of Lake Tahoe (Bureau of Reclamation 2015).

Most of the annual precipitation in the Sierra Nevada falls as snow from November to April, but summer thunderstorms sometimes deliver considerable localized precipitation (Bureau of Reclamation 2015). Peak flows on the Truckee and Carson usually occur in the spring runoff season (April–July) and are driven by snowmelt, and occasional severe winter floods are caused by rain on snow events (Bureau of Reclamation 2015). Climate projections for western North America include as much as a 6°C increase in annual temperature by the year 2100, with a corresponding shift to proportionally more of the annual precipitation as rain (Christensen et al. 2007). An assessment of projections from 12 different climate models suggests an increase of more than 3°C warming in the Truckee Basin (Bureau of Reclamation 2021). Climate observations in the TCRB support

incipient change. Between 1910 and 2008, the average annual temperature at Tahoe City has risen more than 1°C and the percentage of annual precipitation as snow has dropped from 54% to 34% (Bureau of Reclamation 2015).

b. Tree-ring data

A network of 37 chronologies of total width, earlywood width, latewood width, and delta blue intensity from multiple tree species (Table S1 in the online supplemental material) was assembled from the authors' collections and the International Tree-Ring Data Bank (ITRDB 2023). The chronologies are from 21 distinct tree-ring sites in the snow zone (above 1500 m) in the climate footprint of the TCRB (Biondi and Meko 2019) and cover a common period of 1670–1999. Screening for a minimum allowable sample size of 5 cores and expressed population signal (EPS) of 0.85 (Wigley et al. 1984) reduced the network to 31 chronologies and a common period of 1685–1999 (Fig. 1; Table S1). For 6 of the 31 chronologies, the EPS threshold was relaxed to 0.75 to allow better representation of all four variable types and to include two tree species (*Tsuga mertensiana* and *Abies magnifica*) known from previous studies to have a strong snow signal (e.g., Gedalof and Smith 2001; Lepley et al. 2020; Shamir et al. 2020; Littell et al. 2023).

Core indices were calculated by fitting tree-ring measurements with a 100-yr cubic smoothing spline (Cook and Peters 1981) and then dividing the measurements by the fitted curve. Site chronologies were then computed as the biweight mean of the core indices and variance-stabilized, following Osborn et al. (1997), to remove possible variance trend due to changing sample size. These conventional steps of chronology development were implemented using the dendrochronology program library in R (dplR) software package (Bunn 2008). Residual (autocorrelation removed) rather than standard chronologies were preferred for subsequent analysis because the standard chronologies have considerably higher autocorrelation than annual precipitation streamflow records from the TCRB.

c. Climatic data

Global Historical Climate Network (GHCN, version 4) monthly precipitation (Peterson and Vose 1997) and monthly mean temperature (Menne et al. 2018), with the maximum coverage of 1870–2021, were downloaded for 73 precipitation stations and 32 temperature stations in the domain 37.5°–42.0°N and 117°–122°W (Fig. 1; Table S2). These station records were spatially interpolated for later use in WB modeling by inverse distance weighting of standardized anomalies (Jones and Hulme 1996) to 20 WB modeling points distributed over the TCRB at elevations between 1414 and 2779 m (Fig. 2; Table S3). Points were selected with the objective of sampling high, medium, and low elevations in the Truckee and Carson Basins. Eighteen of the points are above the gauges providing natural flows, and both basins are roughly equally represented. Standardized anomalies were computed using station means and standard deviations for the reference period 1941–70. GHCN stations were required to have no more than three (precipitation) or six (temperature) missing years of data in any month of the year in the reference period. Spatial interpolation made use of the nearest m stations ($m \leq 5$) with data and resulted in a continuous record of monthly GHCN P and T for 1870–2021 at each of the 20 modeling points.

The standardized monthly anomalies at the 20 points were converted back to original units of P and T using PRISM data (Daly et al. 2008) means and standard deviations appropriate for the elevations and coordinates of the 20 points. Monthly time series, 1895–2021, for P and T at the 20 model points were downloaded with PRISM explorer (PRISM 2023), and the long-term (1895–2021) monthly means and standard deviations were applied for the conversion. The interpolated GHCN monthly series were then truncated to start with calendar year 1895 to avoid using data from an extremely sparse GHCN station network in subsequent analyses.

d. Hydrologic data

Monthly full natural flow data for the Truckee River at Farad (TRF), California; the East Fork Carson (EFC) River near Gardnerville, Nevada; and West Fork Carson (WFC) River at Woodfords, California (Fig. 2), were downloaded from the California Data Exchange Center (CDEC 2023). These data were summed into totals for the water year (October–September). All three gauges cover water years 1939–2022 but all begin in different years: 1906 for the TRF, 1923 for EFC, and 1939 for WFC. The extremely high interseries correlation ($r > 0.97$; 1939–2022) of these flow records supported statistical extension of the TCRB natural flows back to water year 1906 from subsets of the three gauges (appendix A).

The resulting time series of TCRB water-year natural flow, 1906–2022, referred to from here on as "natural flow," varies greatly on annual and decadal time scales (Fig. 3a). Prominent drought features are extreme single-year low flows in 1924, 1977, and 2021, as well as multiyear droughts in the 1930s and late 1980s to early 1990s. Starting with 1977, the amplitude of highs and lows increases, culminating in the swing from a record high in 2017 to near-record low in 2021.

Descriptive statistics of natural flow differ little between the period with data at all three gauges and earlier years (Table 1). The mean for 1939–2021 (0.9333 billion cubic meters) is 3% higher than the mean for 1906–38. The standard deviation increases by 8% from the earlier to the later period. Natural flows are not significantly autocorrelated in any of the three intervals examined.

e. Water balance modeling

The monthly water balance for a soil column can be written as

$$\mathrm{RO} = P - \mathrm{AET} - \Delta S, \tag{1}$$

where RO is the total runoff, P is the precipitation, AET is the actual evapotranspiration, and ΔS is the change in water storage in the soil and overlying snowpack. The RO in Eq. (1) is assumed to include surface and subsurface runoff.

Time series inputs required by the McCabe–Wolock WB model, which addresses Eq. (1) at a monthly time step, are monthly total P and monthly mean T. A small fraction of the

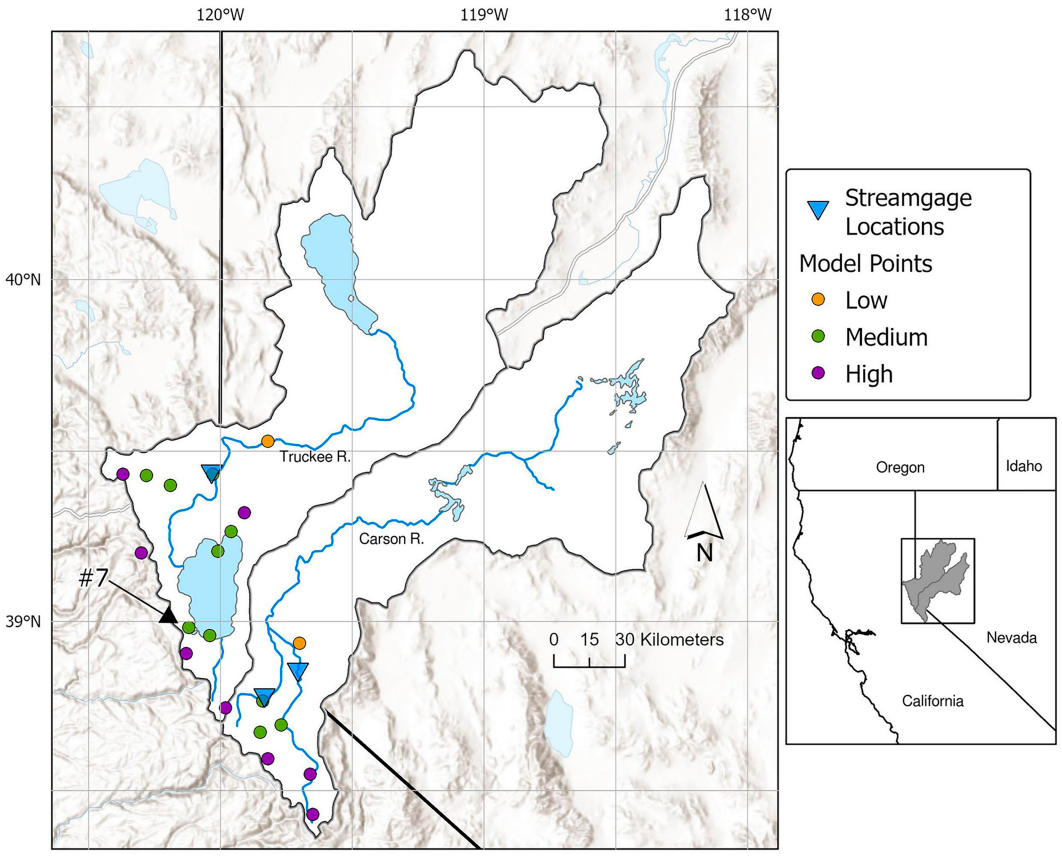

FIG. 2. Stream gauge locations and points for WB modeling. Gauges, from north to south, are TRF, California; EFC near Gardnerville, Nevada; and WFC at Woodfords, California. The 20 modeling points (Table S3) are broadly classified by elevation as high, medium, and low. Point 7 (marked) is the focus of direct and indirect tree-ring reconstruction of runoff.

monthly P is assigned to direct runoff, and the remainder is subject to evapotranspiration from the soil column (Fig. B1). The T influences evapotranspiration through potential evapotranspiration (PET), which is estimated by the Hamon equation (Hamon 1961). The T also affects the fraction of P assigned as snowfall and the rate of melting of the snowpack. The actual evapotranspiration (AET) depends on both PET and the soil moisture. Excess soil moisture (above a specified capacity) becomes surplus runoff.

An important setting in the WB model is the water holding capacity (WHC), which depends on the depth and properties of the soil. The vegetative cover would also be expected to influence WHC because the depth of soil responsive to evapotranspiration depends on rooting depth of plants. Output of the model includes snow accumulation, snowmelt, soil moisture, and runoff. The model equations are described in detail by McCabe and Markstrom (2007) and are not repeated here. Parameter settings specific to our study are given in appendix B.

The WB model was run with P and T input for calendar years 1895–2021 at 20 points distributed over the basin between elevations 2653 and 1414 m (Fig. 2; Table S2). All except two points are above the three stream gauges used to represent the natural flows (Fig. 2). Early calendar years (1895–1904) of model output were discarded because of the sparsity of the climate station network in early years, and to allow for spinup of the WB model from initial conditions (Gray and McCabe 2010). Water years 1906–2021 of model output were used for subsequent analyses.

f. Reconstruction modeling and analysis of reconstructions

Point RO for a selected representative point in the TCRB (point 7 in Fig. 2) was reconstructed from tree-ring chronologies directly and indirectly through a WB model. The predictand y for direct reconstruction is the water-year total of RO output by the WB model from input of observed P and T at point 7. The predictand y for indirect reconstruction of RO is observed seasonal total P and seasonal average mean T. We statistically disaggregate the reconstructed seasonal climate values to monthly values (appendix C) and route those through the WB model to get the indirectly reconstructed RO.

Although the regression predictand y is different for direct and indirect reconstruction, the regression procedure we use is the same. The two-stage procedure, versions of which have

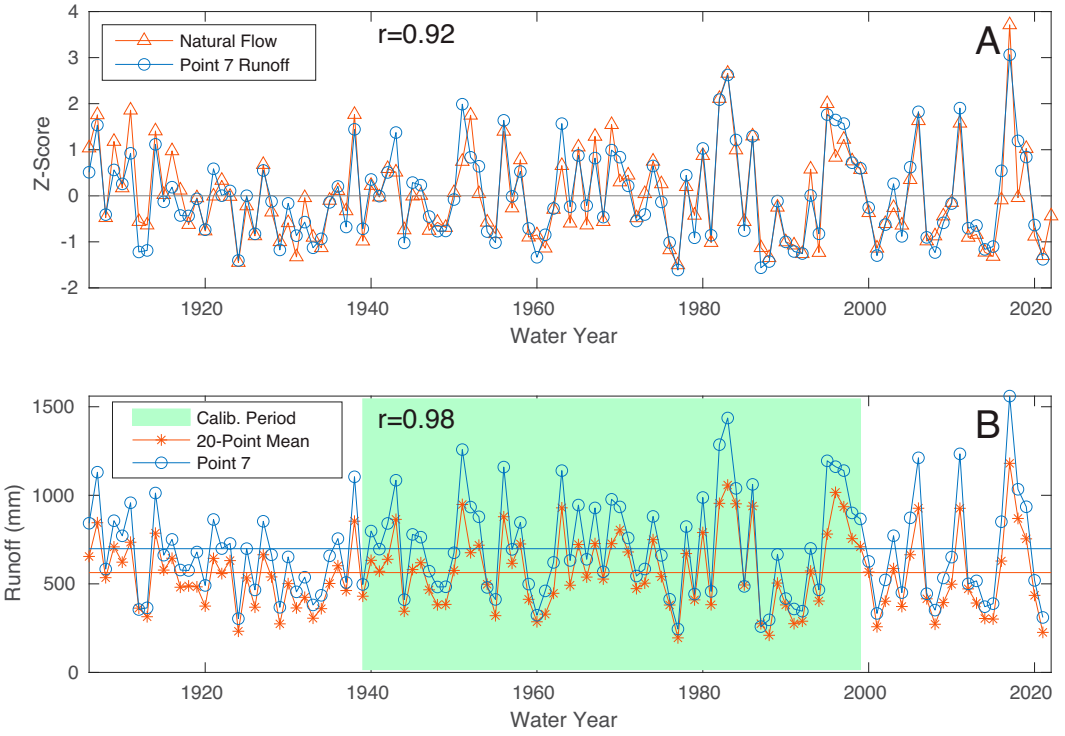

FIG. 3. Runoff history of Truckee–Carson Basin from natural flows and a WB model. (a) Z scores of full natural flow sum for three gauges on Truckee and Carson Rivers and of WB model output runoff at point 7. The Z scores are computed using 1906–2021 means and standard deviations. (b) WB model runoff for point 7 and averaged over 20 points (see Fig. 2). The 1939–99 segment of WB model runoff used for calibration of tree-ring reconstruction models is shaded green. Long-term means, plotted as horizontal lines in (b), and annotated correlations are computed on the common period 1906–2021.

previously been applied in reconstructions of streamflow (e.g., Meko et al. 2001, 2007), is summarized in Fig. 4 and described in detail in appendix D. Stage 1 is stepwise regression of y on lagged tree-ring chronologies to convert each chronology into a separate single-site reconstruction (SSR) of y. Stage 2 is multisite reconstruction (MSR) and consists of stepwise regression of y on principal component (PC) scores of the SSRs to get a final reconstruction model combining information from multiple sites.

TABLE 1. Statistics of the observed full natural flow and model output runoff for subperiods. The statistics are mean, standard deviation, skew, and lag-1 autocorrelation computed for the water year; units are billion cubic meters for flow and millimeters for runoff.

Series[a]	Interval	Mean	Std dev	Skew	$r(1)$
N. flow	1939–99	0.933	0.450	0.49	0.10
	1906–38	0.905	0.415	0.59	0.06
	1906–2021	0.905	0.461	0.87	0.08
Pt-7 RO	1939–99	726.1	290.8	0.36	0.20
	1906–38	658.9	217.0	0.36	−0.06
	1906–2021	698.5	281.4	0.63	0.18
20-pt RO	1939–99	591.7	221.4	0.25	0.24
	1906–38	528.3	162.0	0.16	0.06
	1906–2021	563.6	213.8	0.49	0.24

[a] RO series are for point 7 and averaged over all 20 points (Fig. 2).

The regression approach includes two types of screening intended to emphasize chronologies with a strong signal for y and to lessen the chance of model overfitting. The full set of SSRs is first screened to eliminate chronologies whose models are weak or temporally unstable. Cross validation (Michaelsen 1987) and split-sample validation (Snee 1977) are applied in this screening. The PCs of those SSRs are then screened if necessary to reduce the size of the predictor pool for the MSR regression model. We cap the size of this pool at no more than $N_c/10$ PCs, where N_c is the number of years in the model calibration period, and assign priority in screening to a higher absolute value of correlation of a PC with y.

As an additional safeguard against overfitting, stepwise regressions in stages 1 and 2 apply a cross-validation stopping rule (Wilks 2019) to cut off entry of predictors. Entry is stopped if an additional step would result in the decreased skill of validation as measured by the reduction of error (RE) statistic (Fritts et al. 1990). Further, an early segment of years of y is withheld for independent validation of the reconstruction on data not used in any way for screening chronologies or tuning models. Agreement of reconstructed and observed RO is checked for this period by the Nash–Sutcliffe efficiency (NSE; Nash and Sutcliffe 1970). We conduct an iterative exercise

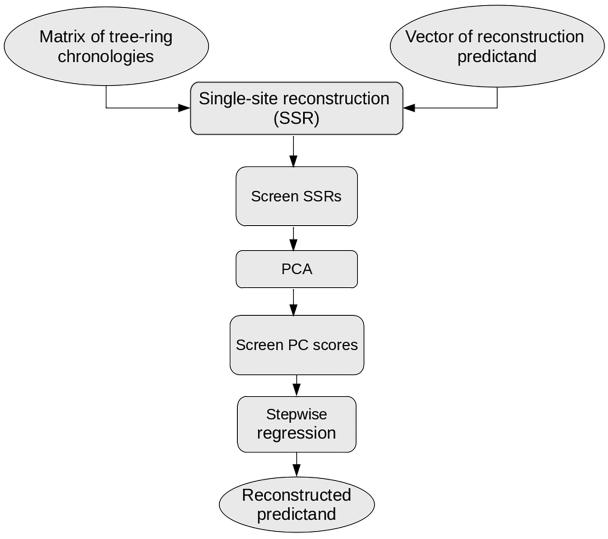

FIG. 4. Sketch illustrating two-stage regression procedure applied in direct and indirect reconstruction. Steps after the estimation of SSR's comprise the MSR, which includes PCA of the SSRs followed by regression with the PC scores as predictors. Both SSR and MSR include loops for cross validation and split-sample validation, as described in the main text and appendix D.

in which the size of the pool of potential predictors for the final model is varied from 1 to $N_c/10$, and we truncate the size of the pool at the step preceding the first drop in NSE.

To emphasize fluctuations at decadal and longer time scales, reconstructions are smoothed using a 15-weight Gaussian filter (Mitchell et al. 1966) with a frequency response of 0.50 at wavelength 17.2 years. Filter weights are listed in Table S4. Applied to a random annual series, this filter gives a similar reduction in variance as a 10-yr running mean. Accordingly, an estimated 95% CI was plotted on the smoothed reconstruction at $\hat{y}_s \pm 1.96\,\mathrm{RMSE}/\sqrt{10}$, where RMSE is the cross-validation root-mean-square error of the annual reconstruction.

One round of two-stage regressions was run for the direct reconstruction of point-7 RO and four rounds for the indirect reconstruction. The predictand for direct reconstruction is the observed model-output RO. The regression predictands for the indirect reconstruction models are total P and average T for the cool and warm seasons October–April and May–September. Reconstructions of seasonal P and T were disaggregated to monthly data needed for WB modeling by partitioning the seasonal values into monthly values proportional to monthly distributions of observed P and T for analog years in the instrumental period (appendix C).

The accuracy of the regression models for reconstruction of RO was summarized with calibration and validation statistics. To facilitate comparison, all models are calibrated and cross validated on the same years, 1939–99. This period is represented by a relatively dense network of climate stations for GHCN interpolation and also by natural flows directly computed from gauged flows (i.e., not extended). The period 1906–38 is held back for a purely independent check of model performance with the NSE. Correlations and time series plots are used to check agreement of direct and indirect reconstructions with each other and with previously published natural flow reconstructions of the Truckee and Carson Rivers. Finally, the indirect reconstruction method is exploited to examine the sensitivity of the relative standing of past droughts to two factors: 1) warming of 3° or 6°C, which is consistent with year-2100 projections for the TCRB (Bureau of Reclamation 2015) and western North America (Christensen et al. 2007); and 2) a radical reduction (halving) of assumed available water capacity. Analyses in this paper were done in a combination of the *R*, MATLAB, and FORTRAN programming environments.

3. Results and discussion

a. *Observed runoff history*

The strong dependence of hydrology on elevation in the TCRB is reflected in the 1906–2021 water-year statistics of WB model input and output at the 20 model points plotted on the map in Fig. 2. Mean P ranges from 1656 mm at the highest point to 239 mm at the low point in Reno. The corresponding RO for those two points is 1229 and 16 mm. For comparison, the mean annual basin runoff computed by dividing the mean annual natural flow by the sum of the areas above the three gauges providing the natural flows (Fig. 2) is 266 mm. Both P and RO are highly spatially correlated, especially at the higher elevations most important to runoff. The median point-to-point correlation is $r = 0.97$ for P and $r = 0.87$ for RO.

Spatial coherence of winter precipitation in the Sierra Nevada explains the high point-to-point correlations noted above. Another likely contributing factor is the inverse-distance interpolation of station P to points; interpolation effectively acts as spatial smoothing of station anomalies. Regardless of the cause, the similarity of times series variations of P and RO at the various model points led us to focus tree-ring reconstruction on a single representative point (point 7) located 2 km off the southwestern shore of Lake Tahoe at an elevation of 2190 m (Fig. 2; Table S2). Scaled for differences in mean and standard deviation, RO at point 7 closely tracks TCRB natural flows (Fig. 3a) as well as RO averaged over all 20 points (Fig. 3b).

b. *Regression*

Regression models for all five predictands—water-year RO and cool-season and warm-season P and T—are statistically significant, explain at least 34% of the predictand variance (adjusted R^2), and have positive skill as measured by cross validation (Table 2; Fig. S1). The number of chronologies contributing to the nonrejected SSR models ranges from 17 for RO to 5 for cool-season T (Table 2). The tree-ring signal is strongest for runoff and cool-season P (adjusted $R^2 > 0.70$), which is reasonable for drought-sensitive trees in a region with a winter-dominant precipitation regime, but for even the weakest model (cool-season T, adjusted $R^2 = 0.34$), the regression is highly significant ($F = 11.5$; $p < 0.0001$; Fig. S1d).

TABLE 2. Calibration and validation statistics of stepwise regression models for reconstruction of RO, seasonal P, and seasonal T at point 7. Statistics are adjusted R^2, reduction-of-error, squared correlation of observed and reconstructed predictand for 1906–38, and the NSE for 1906–38. All models are calibrated and cross validated on 1939–99. All the R^2 values listed represent significant models as measured by the p value for the overall F of regression (see Fig. S1).

Predictand[a]	Screening[b]	R^2	RE	r^2	NSE	Flags[c]
Runoff	17-5-3	0.71	0.70	0.42	0.31	None
Cool-season P	17-5-5	0.72	0.73	0.37	0.31	None
Warm-season P	14-1-1	0.41	0.40	0.28	−0.01	None
Cool-season T	5-3-3	0.34	0.30	0.04	−0.09	None
Warm-season T	10-4-2	0.50	0.49	0.57	0.39	Auto (p = 0.04)

[a] Runoff is water year; seasons are October–April and May–September.
[b] Number of SSRs passing screening, number of PCs of those SSRs in the pool of potential predictors, and number selected by stepwise regression for the final model.
[c] Flags for failure of tests in analysis of residuals, with associated p value for rejection of null hypothesis: residuals were tested (see data and methods) for normality zero lag-1 autocorrelation (Auto), homoskedasticity of variance, and linear trend (Trend).

The skill statistics RE and NSE do not have theoretically based significance tests, but a positive statistic indicates that the reconstruction has lower mean-square error than a null reconstruction consisting of the calibration-period (RE) or validation-period (NSE) observed mean in every year. The five models have positive skill of cross validation (RE > 0) and, except for cool-season T and warm-season P, have positive skill of validation (NSE > 0) on the early period, 1906–38 (Table 2). Observed and reconstructed predictands are significantly correlated ($p < 0.01$) except for the cool-season T model over 1906–38. Given a sample size of 33 years, the critical correlation for significance at $p < 0.01$ is $r = 0.47$ ($r^2 = 0.22$) based on the normal distribution and the estimated variance of a correlation coefficient computed as a function of degrees of freedom (Wilks 2019).

Although all models cross validate, the performance in the held-back years (1906–38), as judged by NSE and r^2, suggests that our tree-ring data have no useful signal for cool-season T and a questionable signal for warm-season P. Analysis of residuals for the five MSR regression models turned up just one flag (Table 2).

The SSR results for warm-season T (10 models accepted) are especially encouraging for indirect RO reconstruction because T in the warm season impacts RO through evapotranspiration. A map of adjusted R^2 for these SSR models shows that chronologies with a significant signal for warm-season T at point 7 are widely scattered, with no obvious geographical proximity to point 7 (Fig. 5). The sign of regression weight on the first predictor to enter stepwise for 8 of the 10 accepted models for warm-season T indicates a negative relationship of T with the tree-ring variable and for the other two models indicates a positive relationship (Table S5). The eight tree-ring chronologies negatively related to warm-season T are width variables (total, earlywood, or latewood) and lags are important in their regression models. Lag $t + 1$ tree-ring index was the first to enter stepwise, with a negative sign, for seven of the eight models. This lag may reflect a snowpack-related growth response: high growth in year $t + 1$ following a deep snowpack and cool summer in year t. This phenomenon has been observed in previous studies (e.g., Lepley et al. 2020; Shamir et al. 2020; Gedalof and Smith 2001).

Delta blue intensity is the tree-ring variable for the two chronologies positively related to warm-season T, and lag-0 was the first lag to enter those models. The strongest warm-season signal in the set of 10 accepted chronologies belongs to delta blue intensity, with the SSR model for one chronology explaining 40% of the variance of warm-season T at point 7 in the 1939–99 calibration period (Fig. S5). Expanded networks of blue-intensity chronologies could be valuable in future studies applying WB modeling to study hydrologic droughts with tree rings in western U.S. basins.

Screening resulted in a widely varying number of PCs in the predictor pools for the MSR stepwise models (Table 2). The NSE computed on data held back from calibration consistently indicated that the predictor pool should be truncated at fewer than six variables. This finding is illustrated with the change in calibration and validation statistics for the RO regression model (Fig. 6). Regression adjusted R^2 and cross-validation RE continue rising to a maximum pool size of 6, but skill of independent verification in the held-back period 1906–38 as measured by NSE peaks at step 5. Similar results were found for the other four regression models, none of which ended up with a predictor pool larger than five (Table 2).

c. *Runoff reconstructions*

Long-term records of tree-ring chronologies, 1685–1999, were substituted into the regression models summarized in Table 2 to get direct and indirect reconstructions of RO with a common period 1688–1999. Indirect reconstruction, unlike direct reconstruction, does not constrain the reconstructed and observed means of y to be equal for the calibration period. The indirect reconstruction of RO has a slight negative bias, −4.4 mm, or less than 1% of the observed 1939–99 mean (726.1 m). We made no bias adjustment to the reconstruction before subsequent time series comparisons and analyses.

The direct and indirect reconstructions closely track one another and are highly correlated ($r = 0.93$) over the 1906–99 period in common to reconstructions and observed model-output RO (Fig. 7). The indirect reconstruction falls outside the 50% confidence interval of the direct reconstruction in 25 of the 94 years 1906–99. The largest departures from the

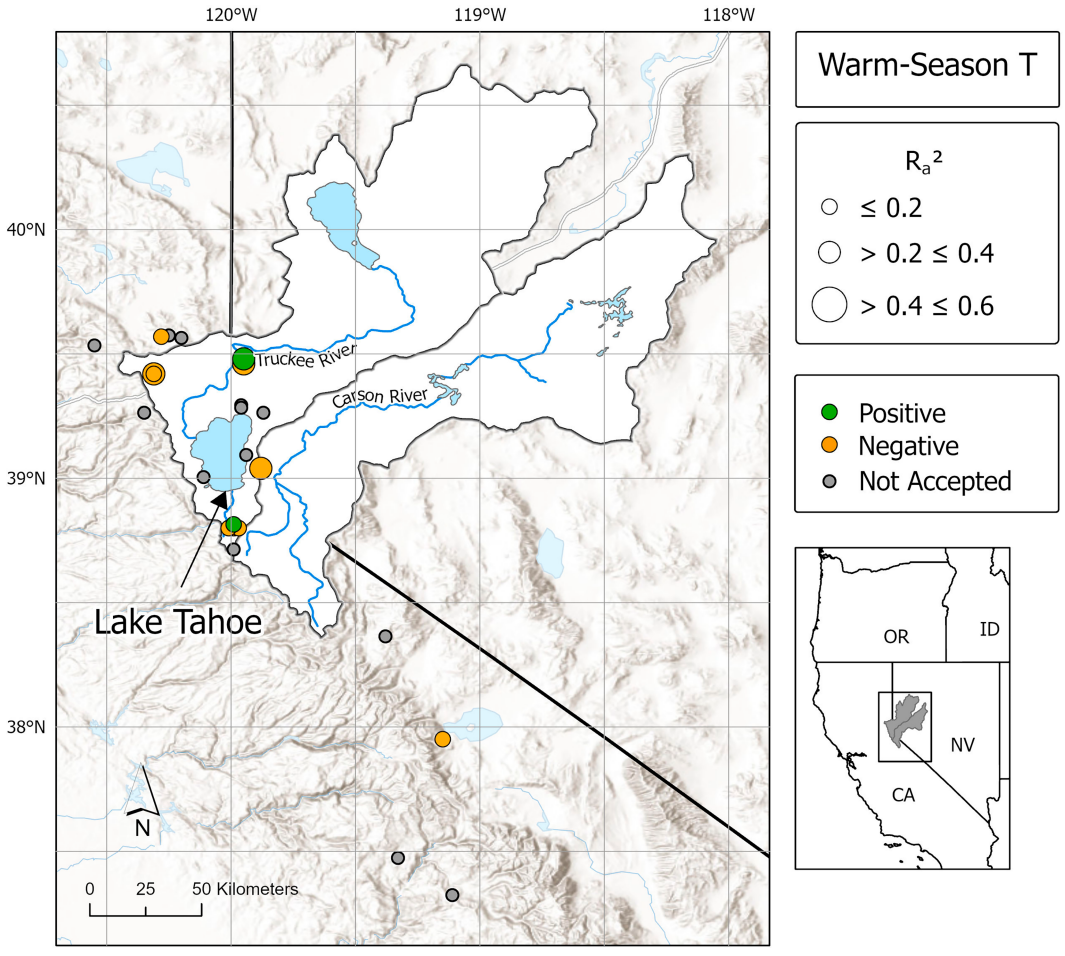

FIG. 5. Map showing chronologies whose SSRs pass screening for reconstruction of warm-season temperature at point 7. Symbols sized proportional to the adjusted R^2 of the SSR model and color coded for the sign of the first predictor to enter the stepwise regression model. Analogous maps for the other four regression predictands (e.g., cool-season P) are included in Fig. S2.

confidence interval are in 1998 on the negative side and in 1984 on the positive side. Both reconstructions are highly correlated ($r \geq 0.79$) with observed RO, 1906–99. The correlation with observed RO is slightly higher ($r = 0.85$, direct; $r = 0.87$, indirect) for the 1939–99 regression calibration period and lower ($r = 0.65$, direct; $r = 0.59$, indirect) for the 1906–38 period withheld from calibration.

Correlations of the observed model with reconstructed runoff as well as the NSE for the held-back years 1906–38 suggest that the direct and indirect reconstructions in this basin are comparably accurate. The NSE slightly favors the direct reconstruction, but conclusions from statistics for the early twentieth century are problematic because the thinning network of climate stations makes the interpolated climate at point 7 more uncertain then (Table S2). Moreover, large year-to-year fluctuations in runoff that would be expected to drive tree-ring responses are less common in 1906–38 than in later years (Fig. 7).

Direct and indirect reconstructions capture isolated single dry years (e.g., 1924) as well as multiyear droughts, such as the three consecutive years of low observed RO in 1959–61 (Fig. 7). The RO anomaly in specific years is sometimes greatly underestimated (e.g., 1977) or overestimated (e.g., 1988). Reconstruction error cannot be eliminated completely because climate is only one of many factors influencing tree growth (Fritts 1976). Moreover, even the observed runoff is inherently uncertain because it was generated by an imperfect hydrologic model whose input is spatially interpolated station climatic data. The relative timing of precipitation and plant processes governing tree growth could be important in amplifying runoff reconstruction errors in particular years. For example, in the 127-yr record of GHCN-interpolated precipitation at point 7 (Table S6), water year 1977 had the record-low October–April precipitation followed by the 13th wettest May–June. The 1977 ring in many trees from our conifer collections in the Sierra Nevada is not unusually narrow. We speculate that the absence of an appreciable snowpack in 1977 was compensated for in some trees by the unusually high precipitation near the start of the period of cambial growth.

Reasons for such large reconstruction errors can perhaps be unraveled by diagnostic studies using daily climatic data

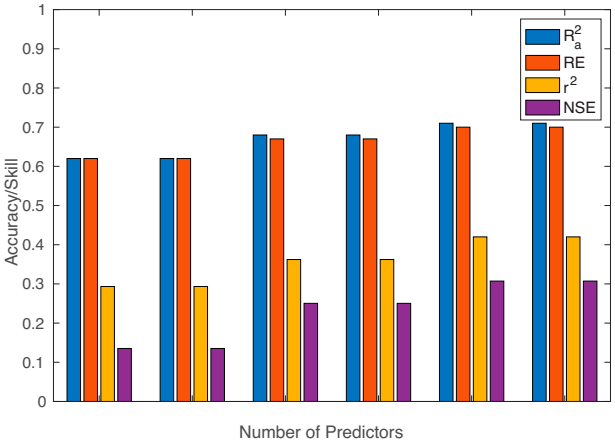

FIG. 6. Change in accuracy and skill of direct runoff reconstruction at point 7 with increasing size of predictor pool. Plotted are the adjusted R^2, the RE statistic from cross validation, the NSE, and the squared correlation of reconstructed runoff with observed runoff. The last two statistics are computed on the held-back period for independent verification (1906–38). The adjusted R^2 and r^2 values plotted represent reconstruction signals significant at $p < 0.01$ (see text and Fig. S1). Skill statistics RE and NSE, while not associated with theoretical significance levels, support positive skill relative to null predictions (see text).

(Jevšenak et al. 2024), process models of tree growth (He et al. 2017), and hydrologic models operating at a daily time step (Shamir et al. 2020). The accuracy of our runoff reconstructions as measured by regression calibration statistics is comparable to that of streamflow reconstructions in the semiarid West from widely varying tree-ring networks and statistical reconstruction approaches (e.g., Meko et al. 2001; Wise 2010; Margolis et al. 2011; Biondi and Meko 2019; Harris and Csank 2023), but errors could possibly be reduced in future studies by expansion of the TCRB tree-ring network to include more chronologies. Errors in dry years could be addressed, for example, with total-width chronologies from the exceptionally precipitation-sensitive blue oak (*Quercus douglasii*) species (Meko et al. 2011), which are below the elevations of deep snowpack but within the climate footprint of the basin (Biondi and Meko 2019). Errors of indirect reconstruction could possibly be reduced by taking advantage of tree-ring variables capable of better resolving seasonal or subseasonal climate anomalies in precipitation and temperature. Our network includes just a few chronologies of subannual width and delta blue intensity. More of these could be developed from existing wood collections for better spatial coverage of the basin. Quantitative wood anatomy might also be explored for improved reconstruction of subseasonally resolved climate inputs (Panyushkina et al. 2003; Gennaretti et al. 2022). A shortcoming of our indirect RO reconstruction model is the lack of an independently verified signal for T variation in the cool season (Table 2). The signal could possibly be improved by allowing the predictor pool for the model to include existing cool-season T reconstructions derived from large-scale tree-ring networks (e.g., Wahl et al. 2014).

Smoothed direct and indirect reconstructions are strongly coherent ($r = 0.91$) over their full length and are broadly consistent with previously published reconstructions (Fig. 8). The twentieth century has lower lows and higher highs than earlier centuries at this level of smoothing. The most prominent extended earlier periods of high and low runoff are centered near 1780 and 1810, respectively. Peaks and troughs in the

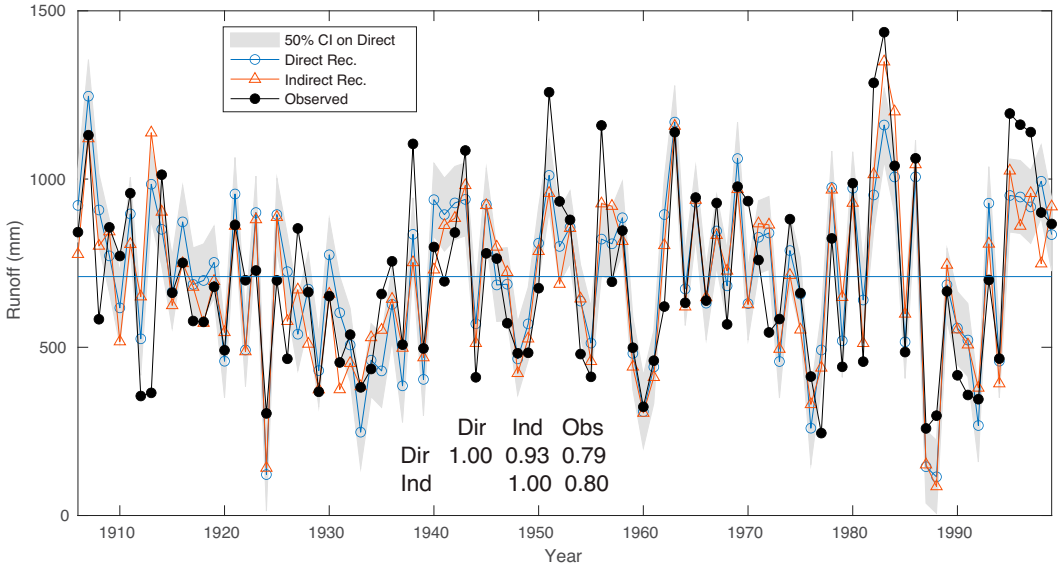

FIG. 7. Tracking of observed point 7 runoff by direct and indirect reconstructions, 1906–99. Confidence interval (50%) of the direct model is plotted at $\hat{y} \pm 0.674\,49$ RMSE, where $\hat{y}$ is the reconstructed runoff and RMSE is the root-mean-square error computed from cross-validation residuals. The horizontal line marks the 1906–99 mean (710 mm) of the direct reconstruction. The correlation matrix for the three plotted series is annotated.

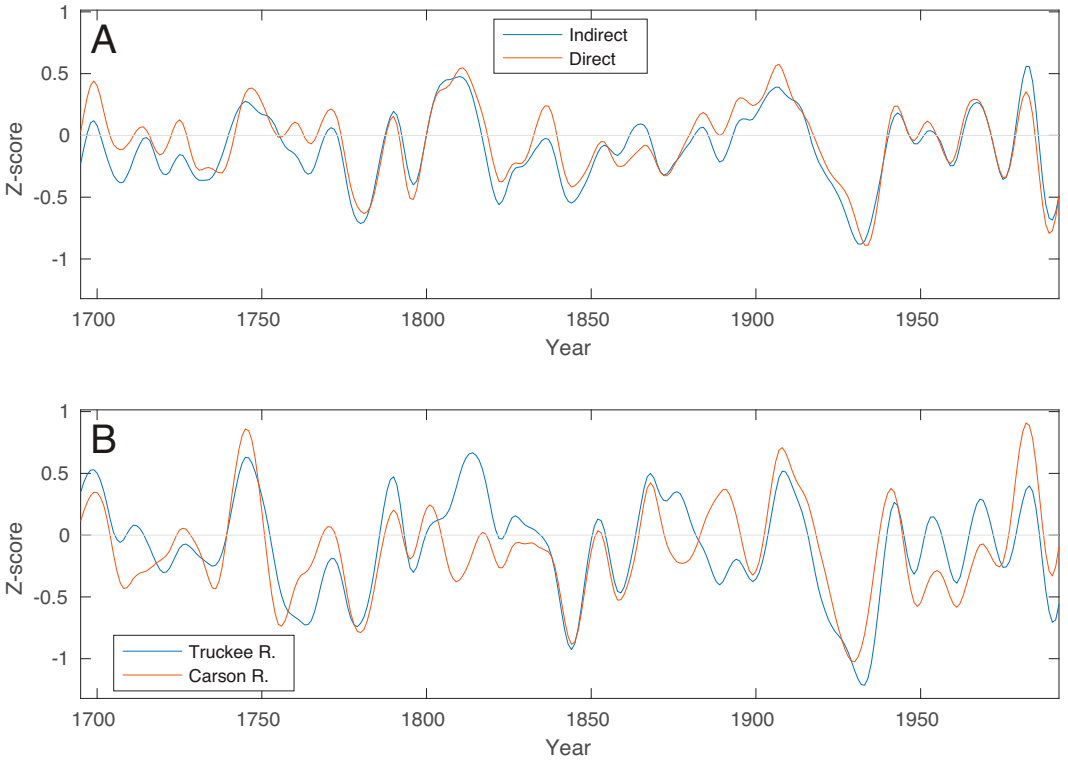

FIG. 8. Consistency of smoothed reconstructed runoff variations for point-7 runoff with other published reconstructions. (a) Direct and indirect reconstructions of point-7 runoff and (b) Z scores of water-year natural-flow reconstruction of Carson River (Harris and Csank 2023) and Truckee River (Biondi and Meko 2019). All series truncated to 1688–1999 before smoothing and converted to Z scores using 1939–99 common-period means and standard deviations. Smoothing by Gaussian filter (weights listed in Table S4). Corresponding annual time series (before smoothing) are plotted in Fig. S3.

direct and indirect reconstructions generally coincide but sometimes differ considerably in amplitude. For example, peaks near 1700 and 1838 are relatively amplified in the direct reconstruction, and troughs near 1707, 1822, and 1844 are relatively amplified in the indirect reconstruction.

A low-frequency feature highlighted by all four reconstructions plotted in Fig. 8 is the unmatched low runoff in the 1930s. Runoff peaks near 1700, 1745, 1907, and 1983 and lows near 1780, 1844, 1933, and 1988 are major features in all four reconstructions. A high in the 1740s and a low in the 1840s are less pronounced in our reconstructions than in the other reconstructions. Differences in reconstructions could arise from use of different forms of the reconstruction statistical model, differences in tree-ring networks, or differences in the target model predictand. Our network is restricted to chronologies in the snow zone of the Sierra Nevada, but the other two reconstructions (Fig. 8b) draw on a broader spatial network of chronologies, including *Quercus douglasii* from lower elevations in California (Meko et al. 2011). Our reconstructions differ from previous reconstructions also in that we include delta blue intensity and subannual width chronologies and lags in the regression models.

The annual series corresponding to the smoothed series plotted in Fig. 8 are also strongly coherent. Direct and indirect reconstructions are significantly correlated with one another ($r = 0.89$; $N = 312$; $p < 0.01$) and with the reconstructions for the Truckee and Carson Rivers (Fig. S3).

d. Drought history comparison

Drought severity was summarized by running means of length 2, 5, 10, and 20 years of reconstructed RO expressed as a percentage of "normal," which we define as the 1939–99 observed mean (726.1 mm). The most severe drought in a particular interval by this measure is the lowest running mean with an ending year in the interval. Droughts of 1688–1905 and 1906–99 serve as a convenient contrast between "twentieth century" and "earlier" droughts because the reliable "observed" model-output RO and the natural flow series for our study both begin with water year 1906.

Maximum drought severity by direct and indirect reconstructions for the twentieth century and earlier years is summarized in Fig. 9. Direct and indirect reconstructions agree the most severe droughts occurred in the twentieth century. This result is consistent with previous tree-ring studies highlighting the severity of twentieth-century droughts in nearby regions in a multicentury context (e.g., Meko et al. 2001, 2011).

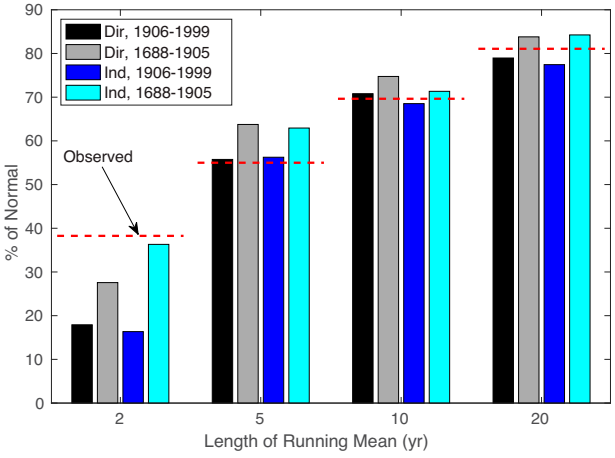

FIG. 9. Three-century context for multiyear droughts by direct and indirect reconstruction of runoff. Lowest running means of length 2, 5, 10, and 20 years for reconstructed water-year runoff at point 7 are plotted for ending years in the twentieth century earlier. Horizontal dashed lines mark the lowest running means in observed runoff, 1906–99.

The indirect reconstruction has slightly lower extremes than the direct reconstruction for three of the four running means, with a maximum difference of 2% for the 10-yr running mean. Lowest running means become less severe with increase in averaging period. For the indirect reconstruction, the low is 16% of normal for 2-yr droughts and 77% of normal for 20-yr droughts.

A closer look at ranked 2- and 10-yr extremes summarized for the 1688–1999 reconstruction shows that the direct and indirect reconstructions identify many of the same droughts but switch the order of severity (Table 3). Six of the eight top-ranking 2-yr droughts and 10-yr droughts in the two reconstructions are the same, although with different ranks. For this assessment, the 10-yr droughts ending in 1829 (direct) and 1831 (indirect) are essentially the same drought because they overlap by 8 years.

Although 1987–88, the extreme 2-yr drought in the direct and indirect reconstructions, is indeed a low in observed RO (Fig. 7), the severity is overestimated in the tree-ring record. This overestimation is also reflected by the position of the horizontal dashed observed line above the lowest bars for 2-yr running means by as much as 22% (Fig. 9). Regression-based reconstructions are generally conservative in that the variance of reconstructed y is less than that of observed y for the calibration period. Reconstructed y anomalies in individual years, however, are not constrained by regression to be less extreme than observed anomalies. The particular overstressing of drought severity in 1988 by these reconstructions may reflect an amplified shock to the trees of one exceptionally dry year following another. Drought legacy, which describes the multiyear impact of drought events on tree growth (Peltier and Ogle 2019; Gazol et al. 2020), has been used to explain the occasional inability of tree-ring chronologies in the TCRB to accurately track "whiplash" events, such as an extremely dry year followed by an extremely wet year (Winitsky et al. 2023).

TABLE 3. Lowest 2- and 10-yr running means of point-7 runoff, 1688–1999, by direct and indirect reconstruction. Ending year of running mean is followed by percentage of normal RO. Normal defined as the observed mean RO (WB output) for the 1939–99 calibration period of the regression model or 726 mm.

	2-yr				10-yr			
	Direct		Indirect		Direct		Indirect	
Rank	Year	%	Year	%	Year	%	Year	%
1	1988	(17.9)	1988	(16.4)	1937	(70.8)	1937	(68.5)
2	1795	(27.6)	1729	(36.3)	1994	(71.6)	1785	(71.3)
3	1777	(45.9)	1777	(37.2)	1785	(74.7)	1994	(72.5)
4	1934	(48.9)	1871	(38.8)	1850	(82.8)	1850	(77.7)
5	1729	(50.7)	1795	(39.4)	1831	(83.0)	1829	(79.5)
6	1783	(51.1)	1783	(48.8)	1802	(83.8)	1737	(80.0)
7	1961	(51.7)	1961	(49.3)	1738	(85.5)	1765	(83.4)
8	1977	(51.7)	1823	(49.4)	1865	(86.6)	1712	(83.8)

e. *Drought sensitivity analysis*

Indirect reconstruction allows the possibility of testing the sensitivity analysis of reconstructed runoff variations to assumed past changes in P, T, or WB model parameters. The sensitivity of the most extreme droughts, 1688–1905, to two scenarios of warming and one of reduced WHC is summarized in Fig. 10. The more extreme warming of 6°C exacerbates the lows in RO by 6%–10%, depending on length of the running mean. Decreasing the WHC by 50% has the opposite effect of lessening the severity of the droughts. The effect of decreased WHC is about a 3%–7% increase in RO, depending on length of moving average. For the longer droughts (10- and 20-yr), halved WHC almost offsets the reduction of RO caused by 6°C warming (Table 4). Although the modeled

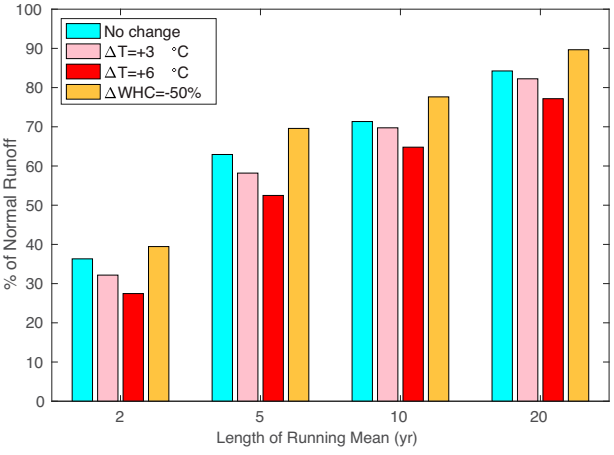

FIG. 10. Sensitivity of most severe indirectly reconstructed drought, 1688–1905, to imposed changes of temperature and WHC. Running means and percentage of normal are as in caption of Fig. 9. The leftmost bar, identical to rightmost bar (light blue) in Fig. 9, is the lowest m-yr mean of reconstructed RO for no change to model inputs or parameters. Next three bars are the corresponding lowest m-yr means for temperature increased (3° and 6°C) and WHC halved to 75 mm from the default 150 mm (orange).

TABLE 4. Impact of warming and reduced WHC on modern context of droughts, 1688–1905.

	RO change[b] (%)		End year	
Length[a]	ΔT	ΔWHC	1906–99[c]	1688–1905[d]
2	−4.1 (−8.9)	3.1	1988	–
5	−4.7 (−10.4)	6.6	1936	1798
10	−1.6 (−6.5)	6.3	1937	1785
20	−2.0 (−7.1)	5.4	1939	1795

[a] Length (year) of running mean.
[b] Change in RO expressed as a percentage of the 1939–99 mean observed RO (726 mm) in response to assumed warming of 3°C (6°C) (T) applied evenly to all months of year, 1688–1905, or assuming halving (to 75 mm) of WHC.
[c] Ending year of lowest reconstructed m-yr mean, 1906–99.
[d] Ending years of m-yr means in 1688–1905 that drop lower than the lowest running mean in 1906–99 because of 6°C imposed warming. No pre-1906 m-yr running means dropped below the lowest observed running mean in 1906–99 in response to a 3°C imposed warming.

impact on RO of such an extreme warming seems slight in terms of percentage of mean RO, 6°C warming applied to the period before the twentieth century would be enough to cause RO anomalies during the most extreme 5-, 10-, and 20-yr droughts in the 1700s to be more severe than those of the twentieth century (Table 4). The milder 3°C warming scenario only slightly (<5%) exacerbates the RO anomaly for running means of the reconstruction, with a decrease of less than 2% in RO for the 10-yr running mean (Fig. 9).

The unexpectedly small decline in modeled running-mean RO during some droughts in response to warming is explained by the impact of warming on the monthly snow regime. This effect is illustrated by the 10-yr period 1776–85, the second ranking low reconstructed running mean of that length according to the indirect reconstruction (Table 3). In that interval, 3°C warming resulted in decreased RO in 6 years and increased RO in 4 years. For the year of largest increased runoff, 1779, the monthly RO, snowmelt, soil water storage, and evapotranspiration are modified such that more P falls as rain instead of snow in the winter and immediately runs off, leaving less water soil water available for loss to evapotranspiration in the later, warmer months of the year (Fig. 11).

Whether full-basin runoff in particular years would have increased in response to 3°C warming would require extension of this sensitivity analysis from a single representative point (point 7) to the full basin, as the snow-regime response to warming would logically vary as a function of elevation and the particular monthly P and T at the location. We acknowledge also that results could change for alternative assumptions of parameter values for the McCabe–Wolock WB model and for alternative hydrologic models (e.g., Shamir et al. 2020; Grogan et al. 2022).

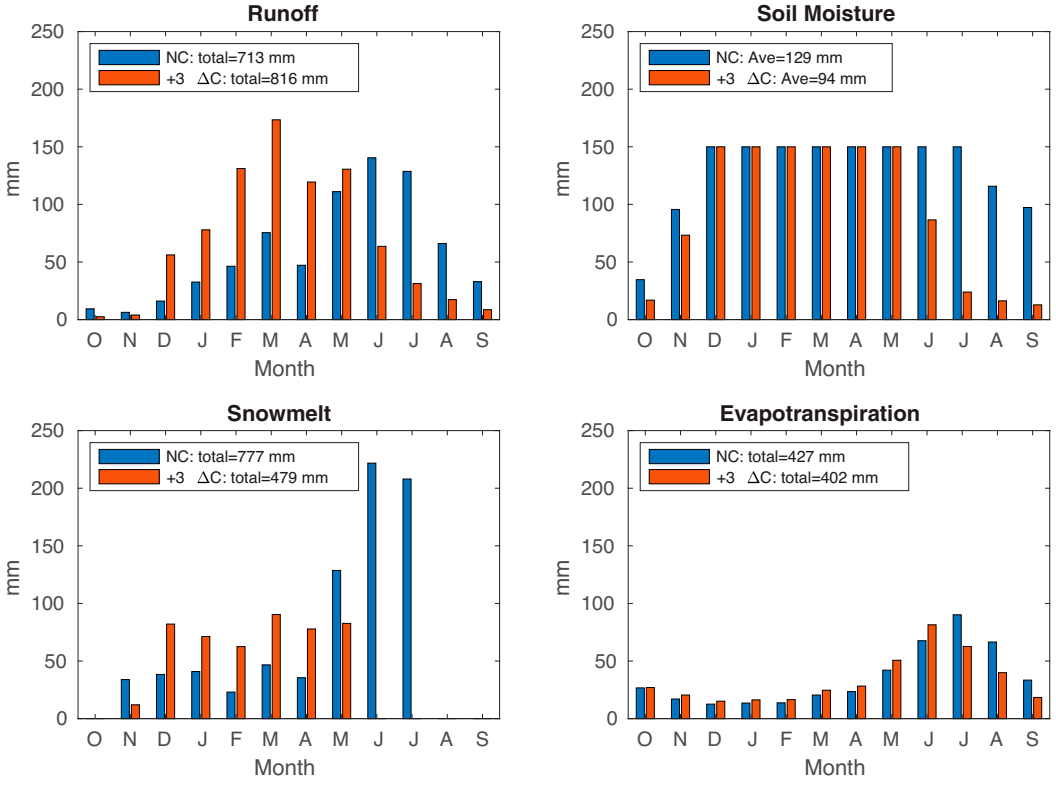

FIG. 11. Monthly indirectly reconstructed RO, snowmelt, soil moisture, and evapotranspiration in water year 1779 with no change (NC) in T and with the imposed warming of 3°C. Input WB-model monthly P and T for the NC scenario in 1779 are plotted in Fig. S4.

The compensation for impacts of warming on RO by warming-related changes in watershed conditions deserves more attention. In our analysis, a 50% reduction in WHC was found to more than offset an imposed warming of 3°C. A more complete sensitivity analysis would associate plausible scenarios of change in WHC and other model parameters with changes in vegetative and soil cover expected with warming. Systematic testing of multiple scenarios is beyond the scope of this paper but should be a focus of future work using WB models and indirect reconstruction.

4. Conclusions

Like many other river basins in the western United States, the TCRB faces water management challenges exacerbated by increasing water demand and climate change. In this paper, water balance (WB) modeling and regression are applied to climatic data and tree-ring chronologies to place runoff variations during severe TCRB droughts in a long-term context. Results, consistent across reconstruction approaches, indicate that extreme multiyear droughts of the twentieth century are unmatched in severity back to at least the late 1600s and suggest that a temperature increase of 3°C superimposed on the past would actually have yielded a slight increase in annual runoff in some years of past severe extended droughts because of a changing snowmelt regime.

Runoff reconstruction in the TCRB through a monthly WB model was possible with a limited available network of tree-ring chronologies of various data types, including delta blue intensity. Future studies would benefit from tree-ring data with improved temporal resolution of P and T anomalies and from extension of chronologies to cover droughts of the more distant past (e.g., late 1500s) and the twenty-first century. Given the importance of a changing snowmelt regime to the runoff response to regional warming, an improved tree-ring signal for cool-season T would be especially valuable. Runoff reconstruction through WB models could find water resource applications in other river basins, especially those lacking long-time series of natural flow or whose gauged streamflow records are distorted by dams and other human influence. Whether part of the runoff reconstruction process itself, as in this study, or as a complementary diagnostic tool, WB modeling can contribute to a better understanding of the climatic signatures of droughts and wet periods in the tree-ring record.

Acknowledgments. This work was supported by National Science Foundation Awards 1903535 and 1903561 from the P2C2 Program and Awards 1917503 and 1917515 from the Office of Polar Programs. We thank Greg McCabe for providing the FORTRAN code for the water balance model and Landon Breeding for invaluable assistance in preparation of maps.

Data availability statement. Newly developed tree-ring chronologies and reconstructions will be submitted to the International Tree-Ring Data Bank (ITRDB 2023), managed by the World Data Service for Paleoclimatology, following publication of this paper. The submission to the ITRDB will include a file, ReconAnalogTCRB.zip, with R software for the two-stage regression modeling with data sufficient to duplicate our regression results. The software was written in support of a web-based dendrohydrology reconstruction tool, Tree-Ring Integrated System for Hydrology (TRISH), being developed for use with the University of New Hampshire water balance model (Panyushkina et al. 2023). The aforementioned data and software as well as additional supplemental material can be accessed at the University of Arizona Research Data Repository (https://doi.org/10.25422/azu.data.25541590).

APPENDIX A

Extension of Natural Flows

This appendix describes the statistical extension of the TCRB natural flows (three-gauge sum) from 1939 to 2022 back to 1906 from gauges with data before 1939. The natural flows for TRF, EFC, and WFC (Fig. 2) have starting years 1906, 1923, and 1939. The extension was made using time series of natural flow summed over the water year.

Assume a predictor series x, a predictand series y requiring extension, an observation y_i in a specific year i requiring estimation, and a value x_i of the predictor series in year i. Further, define C as a reference period during which both x and y have data. The following quantile-analog method was used for estimation: The time series x and y for period C are sorted, the quantile of x_i in C is determined by linear interpolation, and the same quantile of y in C is used as the estimate of y_i. This method was applied to extend WFC back to 1923 from predictor EFC and to extend both WFC and EFC over 1906–22 using predictor TRF. After extension of the individual records, the TCRB natural flow series, water years 1906–2022, was computed as the sum of EFC + WFC + TRF.

APPENDIX B

Water Balance Model

This appendix contains additional details about the WB modeling. The FORTRAN code for the WB model was obtained from Greg McCabe (U.S. Geological Survey 2015, personal communication) and was compiled and run on a laptop with a Linux (Ubuntu) operating system using the GNU FORTRAN 11.4.0 compiler. The model (Fig. B1) runs at a monthly time step. We used the default program settings of model parameters, listed below. For ease of reference, we use the same abbreviations for WB model terms as McCabe and Markstrom (2007):

1) WHC = 150 mm; water holding capacity of the soil (soil moisture storage capacity)
   Excess of soil moisture storage S above WHC in the monthly accounting is allocated to runoff (RO). It is necessary to assume an S at the start of the accounting

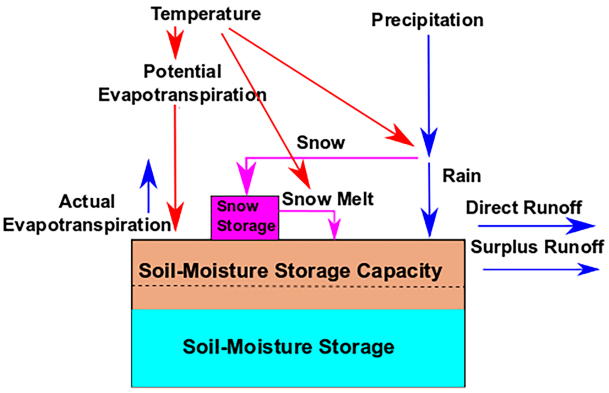

FIG. B1. Simplified sketch of the WB model. Figure adapted from McCabe and Markstrom (2007).

(January of first year). The WB output for several years after that can be distorted by incorrect specification of initial S (Gray and McCabe 2010). Our input monthly precipitation P and temperature T data start in January 1895, but we do not begin interpreting model output until water year 1906. We assume initial saturation (S = 150 mm), which might be reasonable in the Sierra Nevada. If WHC is exceeded in the monthly accounting, the excess is assigned as "surplus." For the sensitivity exercise, the water holding capacity was halved, WHC = 75 mm.

2) *tsnow* = −4.0°C; threshold T for snow
   Below this threshold of monthly mean T, all P is snow, or P_{snow}.
3) *train* = 7.0°C; threshold T for rain
   Above this threshold of monthly mean T, all P is rain, or P_{rain}. Between a monthly mean T of *train* and *tsnow*, the fraction of P as P_{rain} varies linearly in proportion to the fraction $(T - tsnow)/(train - tsnow)$.
4) *directfac* = 0.05; decimal fraction of P_{rain} to direct runoff
   This small fraction of total P_{rain} is assumed to immediately (same month) contribute to direct RO rather than to enter into the water balance of the soil column, no matter how dry that soil is.
5) *rfactor* = 0.50; runoff factor
   The decimal fraction of surplus assigned to RO. All of the surplus computed for a month is not assigned to RO in that same month but is gradually released according to this rule.
6) *xmeltcoeff* = 0.47; daily melt coefficient
   This coefficient along with the difference $T - T_{\text{snow}}$ determines what fraction of the snow water storage is assigned to snowmelt runoff in the month. [Notation here is taken from the FORTRAN program rather than McCabe and Markstrom (2007).] The snowmelt is computed as $xmelt = xmeltcoeff(T - T_{\text{snow}})N$, where N is the number of days in the month. This equation can yield an *xmelt* greater than the actual snow water storage, and in that case, the entire snowpack is assumed to melt (i.e., *xmelt* cannot exceed the existing snow water storage).

APPENDIX C

Temporal Disaggregation of Reconstructed Seasonal *P* and *T*

Temporal disaggregation in this paper is defined as the conversion of a tree-ring reconstruction of seasonal total P or seasonal average T into the monthly values needed as input to the WB model for indirect reconstruction of runoff. This appendix describes the analog method adopted for disaggregation. Let $\hat{y}_t$ be the reconstructed seasonal P, say, covering water years 1688–1999, designated here as period B. Assume that observed y and its monthly values are available for a recent interval A, 1901–99, which overlaps B. Further, let $\hat{y}_k$ be the reconstructed seasonal P for some year prior to A. For P, the analog method assigns the same monthly proportions of seasonal p as the observed monthly proportions in the "analog" year, defined as the year t in A with $\hat{y}_t$ closest to $\hat{y}_k$. For T, the monthly means in the analog year are shifted by some constant (same for all months) so that the seasonal average is the same as in the reconstruction year.

APPENDIX D

Two-Stage Regression

This appendix lists the steps in reconstruction of a predictand y from tree-ring data by two-stage regression. The same form of model applies to the indirect and direct reconstructions of point-7 annual (water year) runoff generated in this paper. For direct reconstruction, y is the model output RO from a water balance model using observed precipitation P and temperature T as model input. For indirect reconstruction, y is either seasonal total observed P or seasonal average T. Supplemental material ReconAnalogTCRB.zip contains all input data, R scripts, and R functions needed to carry out the regression modeling described in the main paper.

1) Regress y_t stepwise forward on the pool of five potential predictors consisting of x_t lagged −2 years to +2 years from y_t, where x is a residual tree-ring chronology and the subscript t is a year. As each predictor enters, cross validate the model by leave-nine-out cross validation—preserves independence of calibration and validation sets when model includes lags (Meko 1997). Entry is stopped if next step fails to yield an increase in validation skill as measured by the reduction of error (RE) statistic (Fritts et al. 1990). All models in this paper were calibrated on the years 1939–99 of y, except for the special case of positive lags in the final model and tree-ring data ending in 1999. In that case, the calibration period was necessarily shortened to 1939–98 or 1939–97, depending on how many positive lags.
2) Split the full calibration period in half and recalibrate the model from the previous step on the first half and validate on the second half and then exchange the calibration and validation halves. Record the skill of split-sample validation by the RE statistic for each half.

3) Accept the model from step 1, only if the following four conditions are satisfied: 1) full-period calibration is statistically significant ($p \leq 0.05$ for regression overall-F), 2) full-period model has skill (RE > 0) as measured by cross validation, 3) both split-sample calibrations yield positive RE, and 4) the final model is physically logical in that at least one of the lagged predictors is nonnegative. This last condition eliminates models that imply the current year's P, say, can be predicted from past year's tree-ring index.
4) Repeat steps 1–3 for all 31 tree-ring chronologies, resulting in $N_1 \leq 31$ single-site models passing screening.
5) Apply the N_1 regression models to the long-term tree-ring chronologies to generate N_1 single-site reconstructions.
6) Run a principal component analysis (PCA) on the common-period matrix of the N_1 SSRs. The PCA is run on the covariance matrix of the SSRs because variance differences among the SSRs are important. A high variance reflects a strong signal for y in the chronology. The PCA yields N_1 principal components (PCs) and a time series matrix of N_1 PC scores.
7) Screen the matrix of PC scores, if needed, so that it includes just the N_2 PCs most highly correlated (absolute) with y if needed so that only the $N_2 \leq N_1$ most highly correlated (absolute value) with y are retained. As a safeguard against chance relationships and overfitting, only the $N_2 \leq N_c/10$ highest correlated PCs are retained, where N_c is the number of years in the regression model calibration period. As described in the paper, we repeat regression analyses with N_2 varying from 1 to $N_c/10$ and truncate the size of the pool at the smallest size giving the maximum NSE when the model is applied to predict y for the held-back period 1906–38.
8) Regress y forward stepwise on the PC scores from the preceding step to get the final or multisite reconstruction (MSR) model. Again, as with the SSR models, a cross-validation (leave-nine-out) stopping rule is applied to avoid adding predictors that do not increase validation skill.
9) Substitute the long-term PC scores into the MSR model to generate the final reconstruction.

REFERENCES

Allen, C. D., and Coauthors, 2010: A global overview of drought and heat-induced tree mortality reveals emerging climate change risks for forests. *For. Ecol. Manage.*, **259**, 660–684, https://doi.org/10.1016/j.foreco.2009.09.001.

Babst, F., W. E. Wright, P. Szejner, L. Wells, S. Belmecheri, and R. K. Monson, 2016: Blue intensity parameters derived from Ponderosa pine tree rings characterize intra-annual density fluctuations and reveal seasonally divergent water limitations. *Trees*, **30**, 1403–1415, https://doi.org/10.1007/s00468-016-1377-6.

Bégin, Y., 2001: Tree-ring dating of extreme lake levels at the Subarctic–Boreal interface. *Quat. Res.*, **55**, 133–139, https://doi.org/10.1006/qres.2000.2203.

Biondi, F., and S. Strachan, 2012: Dendrohydrology in 2050: Challenges and opportunities. *Toward a Sustainable Water Future: Visions for 2050*, W. M. Grayman, D. P. Loucks, and L. Saito, Eds., American Society of Civil Engineers, 355–362.

——, and D. M. Meko, 2019: Long-term hydroclimatic patterns in the Truckee-Carson basin of the eastern Sierra Nevada, USA. *Water Resour. Res.*, **55**, 5559–5574, https://doi.org/10.1029/2019WR024735.

Brito-Castillo, L., S. Díaz-Castro, C. A. Salinas-Zavala, and A. V. Douglas, 2003: Reconstruction of long-term winter streamflow in the Gulf of California continental watershed. *J. Hydrol.*, **278**, 39–50, https://doi.org/10.1016/S0022-1694(03)00131-8.

Bunn, A. G., 2008: A dendrochronology program library in R (dplR). *Dendrochronologia*, **26**, 115–124, https://doi.org/10.1016/j.dendro.2008.01.002.

Bureau of Reclamation, 2015: Truckee basin study, basin study report. Reclamation: Managing Water in the West, accessed 26 August 2023, https://www.usbr.gov/watersmart/bsp/docs/finalreport/truckee/tbsbasinstudy.pdf.

——, 2021: Truckee and Carson River basins, SECURE water act section 9503(c), report to congress. Accessed 26 August 2023,https://www.usbr.gov/climate/secure/docs/2021secure/basinreports/TruckeeBasinChapter.pdf.

Cayan, D. R., K. T. Redmond, and L. G. Riddle, 1999: ENSO and hydrological extremes in the western United States. *J. Climate*, **12**, 2881–2893, https://doi.org/10.1175/1520-0442(1999)012<2881:EAHEIT>2.0.CO;2.

CDEC, 2023: California Data Exchange Center. California Department of Water Resources, accessed 12 May 2023, http://cdec.water.ca.gov/index.html.

Chen, F., and Coauthors, 2022: Ecological and societal effects of Central Asian streamflow variation over the past eight centuries. *npj Climate Atmos. Sci.*, **5**, 27, https://doi.org/10.1038/s41612-022-00239-5.

Christensen, J. H., and Coauthors, 2007: Regional climate projections. *Climate Change 2007: The Physical Science Basis*, S. Solomon et al., Eds., Cambridge University Press, 848–940.

Cook, E. R., and K. Peters, 1981: The smoothing spline: A new approach to standardizing forest interior tree-ring width series for dendroclimatic studies. *Tree-Ring Bull.*, **41**, 45–53.

——, C. A. Woodhouse, C. M. Eakin, D. M. Meko, and D. W. Stahle, 2004: Long-term aridity changes in the western United States. *Science*, **306**, 1015–1018, https://doi.org/10.1126/science.1102586.

Daly, C., M. Halbleib, J. I. Smith, W. P. Gibson, M. K. Doggett, G. H. Taylor, J. Curtis, and P. P. Pasteris, 2008: Physiographically sensitive mapping of climatological temperature and precipitation across the conterminous United States. *Int. J. Climatol.*, **28**, 2031–2064, https://doi.org/10.1002/joc.1688.

Fritts, H. C., 1976: *Tree Rings and Climate*. Academic Press, 567 pp.

——, J. Guiot, and G. A. Gordon, 1990: Verification. *Methods of Dendrochronology: Applications in the Environmental Sciences*, E. R. Cook and L. A. Kairiukstis, Eds., Kluwer Academic Publishers, 178–185.

Gangopadhyay, S., G. J. McCabe, and C. A. Woodhouse, 2015: Beyond annual streamflow reconstructions for the Upper Colorado River Basin: A paleo-water-balance approach. *Water Resour. Res.*, **51**, 9763–9774, https://doi.org/10.1002/2015WR017283.

Garfin, G., A. Jardine, R. Merideth, M. Black, and S. LeRoy, 2013: *Assessment of Climate Change in the Southwest United States*. Island Press, 508 pp., https://doi.org/10.5822/978-1-61091-484-0.

Gazol, A., and Coauthors, 2020: Drought legacies are short, prevail in dry conifer forests and depend on growth variability.

J. Ecol., **108**, 2473–2484, https://doi.org/10.1111/1365-2745.13435.

Gedalof, Z., and D. J. Smith, 2001: Dendroclimatic response of mountain hemlock (*Tsuga mertensiana*) in Pacific North America. *Can. J. For. Res.*, **31**, 322–332, https://doi.org/10.1139/x00-169.

Gennaretti, F., M. Carrer, I. García-González, S. Rossi, and G. von Arx, 2022: Editorial: Quantitative wood anatomy to explore tree responses to global change. *Front. Plant Sci.*, **13**, 998895, https://doi.org/10.3389/fpls.2022.998895.

Gray, S. T., and G. J. McCabe, 2010: A combined water balance and tree ring approach to understanding the potential hydrologic effects of climate change in the central Rocky Mountain region. *Water Resour. Res.*, **46**, W05513, https://doi.org/10.1029/2008WR007650.

——, C. L. Fastie, S. T. Jackson, and J. L. Betancourt, 2004: Tree-ring-based reconstruction of precipitation in the Bighorn Basin, Wyoming, since 1260 A.D. *J. Climate*, **17**, 3855–3865, https://doi.org/10.1175/1520-0442(2004)017<3855:TROPIT>2.0.CO;2.

Griffin, D., D. M. Meko, R. Touchan, S. W. Leavitt, and C. A. Woodhouse, 2011: Latewood chronology development for summer-moisture reconstruction in the US Southwest. *Tree-Ring Res.*, **67**, 87–101, https://doi.org/10.3959/2011-4.1.

Grogan, D. S., S. Zuidema, A. Prusevich, W. M. Wollheim, S. Glidden, and R. B. Lammers, 2022: Water balance model (WBM) v.1.0.0: A scalable gridded global hydrologic model with water-tracking functionality. *Geosci. Model Dev.*, **15**, 7287–7323, https://doi.org/10.5194/gmd-15-7287-2022.

Hamon, W. R., 1961: Estimating potential evapotranspiration. *J. Hydraul. Div.*, **87**, 107–120, https://doi.org/10.1061/JYCEAJ.0000599.

Harris, V. M., and A. Z. Csank, 2023: A new 500-year reconstruction of Truckee River streamflow. *Dendrochronologia*, **79**, 126093, https://doi.org/10.1016/j.dendro.2023.126093.

He, M., V. Shishov, N. Kaparova, B. Yang, A. Bräuning, and J. Grießinger, 2017: Process-based modeling of tree-ring formation and its relationships with climate on the Tibetan Plateau. *Dendrochronologia*, **42**, 31–41, https://doi.org/10.1016/j.dendro.2017.01.002.

Heeter, K. J., G. L. Harley, J. T. Maxwell, R. J. Wilson, J. T. Abatzoglou, S. A. Rayback, M. L. Rochner, and K. A. Kitchens, 2021: Summer temperature variability since 1730 CE across the low-to-mid latitudes of western North America from a tree ring blue intensity network. *Quat. Sci. Rev.*, **267**, 107064, https://doi.org/10.1016/j.quascirev.2021.107064.

Hu, M., and Coauthors, 2023: Climate change increases the instability of the water supply for hydropower stations on the Tibetan Plateau. *Environ. Res. Lett.*, **18**, 114040, https://doi.org/10.1088/1748-9326/ad0311.

ITRDB, 2023: Tree rings. Accessed 1 July 2022,https://www.ncei.noaa.gov/products/paleoclimatology/tree-ring.

Jevšenak, J., A. Buras, and F. Babst, 2024: Shifting potential for high-resolution climate reconstructions under global warming. *Quat. Sci. Rev.*, **325**, 108486, https://doi.org/10.1016/j.quascirev.2023.108486.

Jones, P. D., and M. Hulme, 1996: Calculating regional climate time series for temperature and precipitation: Methods and illustrations. *Int. J. Climatol.*, **16**, 361–377, https://doi.org/10.1002/(SICI)1097-0088(199604)16:4<361::AID-JOC53>3.0.CO;2-F.

Kleppe, J. A., D. S. Brothers, G. M. Kent, F. Biondi, S. Jensen, and N. W. Driscoll, 2011: Duration and severity of Medieval drought in the Lake Tahoe Basin. *Quat. Sci. Rev.*, **30**, 3269–3279, https://doi.org/10.1016/j.quascirev.2011.08.015.

Klos, P. Z., T. E. Link, and J. T. Abatzoglou, 2014: Extent of the rain-snow transition zone in the western U.S. under historic and projected climate. *Geophys. Res. Lett.*, **41**, 4560–4568, https://doi.org/10.1002/2014GL060500.

Lepley, K., R. Touchan, D. Meko, E. Shamir, R. Graham, and D. Falk, 2020: A multi-century Sierra Nevada snowpack reconstruction modeled using upper-elevation coniferous tree rings (California, USA). *Holocene*, **30**, 1266–1278, https://doi.org/10.1177/0959683620919972.

Littell, J. S., G. T. Pederson, J. T. Martin, and S. T. Gray, 2023: Networks of tree-ring based streamflow reconstructions for the Pacific Northwest, U.S.A. *Water Resour. Res.*, **59**, e2023WR035255, https://doi.org/10.1029/2023WR035255.

Lutz, E. R., A. F. Hamlet, and J. S. Littell, 2012: Paleoreconstruction of cool season precipitation and warm season streamflow in the Pacific Northwest with applications to climate change assessments. *Water Resour. Res.*, **48**, W01525, https://doi.org/10.1029/2011WR010687.

MacDonald, G. M., and Coauthors, 2008: Climate warming and 21st-century drought in southwestern North America. *Eos, Trans. Amer. Geophys. Union.*, **89**, 82, https://doi.org/10.1029/2008EO090003.

Margolis, E. Q., D. M. Meko, and R. Touchan, 2011: A tree-ring reconstruction of streamflow in the Santa Fe River, New Mexico. *J. Hydrol.*, **397**, 118–127, https://doi.org/10.1016/j.jhydrol.2010.11.042.

McCabe, G. J., and S. L. Markstrom, 2007: A monthly water-balance model driven by a graphical user interface. U.S. Geological Survey Open-File Rep. 2007–1088, 6 pp.

——, and D. M. Wolock, 2007: Warming may create substantial water supply shortages in the Colorado River basin. *Geophys. Res. Lett.*, **34**, L22708, https://doi.org/10.1029/2007GL031764.

——, M. A. Palecki, and J. L. Betancourt, 2004: Pacific and Atlantic Ocean influences on multidecadal drought frequency in the United States. *Proc. Natl. Acad. Sci. USA*, **101**, 4136–4141, https://doi.org/10.1073/pnas.0306738101.

——, J. L. Betancourt, S. T. Gray, M. A. Palecki, and H. G. Hidalgo, 2008: Associations of multi-decadal sea-surface temperature variability with US drought. *Quat. Int.*, **188**, 31–40, https://doi.org/10.1016/j.quaint.2007.07.001.

Meko, D., 1997: Dendroclimatic reconstruction with time varying predictor subsets of tree indices. *J. Climate*, **10**, 687–696, https://doi.org/10.1175/1520-0442(1997)010<0687:DRWTVP>2.0.CO;2.

Meko, D. M., and C. A. Woodhouse, 2011: Application of streamflow reconstruction to water resources management. *Dendroclimatology, Progress and Prospects*, M. K. Hughes, T. W. Swetnam, and H. F. Diaz, Eds., Springer Science+Business Media B.V., 231–261.

——, M. D. Therrell, C. H. Baisan, and M. K. Hughes, 2001: Sacramento River flow reconstructed to A.D. 869 from tree rings. *J. Amer. Water Resour. Assoc.*, **37**, 1029–1039, https://doi.org/10.1111/j.1752-1688.2001.tb05530.x.

——, C. A. Woodhouse, C. A. Baisan, T. Knight, J. J. Lukas, M. K. Hughes, and M. W. Salzer, 2007: Medieval drought in the upper Colorado River Basin. *Geophys. Res. Lett.*, **34**, L10705, https://doi.org/10.1029/2007GL029988.

——, D. W. Stahle, D. Griffin, and T. A. Knight, 2011: Inferring precipitation-anomaly gradients from tree rings. *Quat. Int.*, **235**, 89–100, https://doi.org/10.1016/j.quaint.2010.09.006.

——, C. A. Woodhouse, and K. Morino, 2012: Dendrochronology and links to streamflow. *J. Hydrol.*, **412–413**, 200–209, https://doi.org/10.1016/j.jhydrol.2010.11.041.

——, R. Touchan, D. Kherchouche, and S. Slimani, 2020: Direct versus indirect tree-ring reconstruction of annual discharge of Chemora River, Algeria. *Forests*, **11**, 986, https://doi.org/10.3390/f11090986.

Menne, M. J., C. N. Williams, B. E. Gleason, J. J. Rennie, and J. H. Lawrimore, 2018: The Global Historical Climatology Network monthly temperature dataset, version 4. *J. Climate*, **31**, 9835–9854, https://doi.org/10.1175/JCLI-D-18-0094.1.

Michaelsen, J., 1987: Cross-validation in statistical climate forecast models. *J. Climate Appl. Meteor.*, **26**, 1589–1600, https://doi.org/10.1175/1520-0450(1987)026<1589:CVISCF>2.0.CO;2.

Millar, C. I., and N. L. Stephenson, 2015: Temperate forest health in an era of emerging megadisturbance. *Science*, **349**, 823–826, https://doi.org/10.1126/science.aaa9933.

Mitchell, J. M., Jr., B. Dzerdzeevskii, H. Flohn, W. L. Hofmeyr, H. H. Lamb, K. N. Rao, and C. C. Wallén, 1966: Climatic change. WMO Tech. Note 79, 81 pp.

Nash, J. E., and J. V. Sutcliffe, 1970: River flow forecasting through conceptual models. Part I—A discussion of principle. *J. Hydrol.*, **10**, 282–290, https://doi.org/10.1016/0022-1694(70)90255-6.

National Research Council, 2006: *Surface Temperature Reconstructions for the Last 2000 Years*. The National Academy Press, 160 pp.

Osborn, T. J., K. R. Briffa, and P. D. Jones, 1997: Adjusting variance for sample-size in tree-ring chronologies and other regional mean timeseries. *Dendrochronologia*, **15**, 89–99.

Panyushkina, I., D. Meko, R. Thaxton, A. I. Shiklomanov, A. Prusevich, S. Glidden, and R. Lammers, 2023: Assessment of Arctic warming impact on Siberian hydrology using online tool TRISH: Tree-Ring Integrated System for Hydrology. *TRACE 2023—Tree Rings in Archaeology, Climatology and Ecology*, Coimbra, Portugal, MedDendro, 230–231, https://www.uc.pt/site/assets/files/1067994/abstract_book_trace_2023.pdf.

Panyushkina, I. P., M. K. Hughes, E. A. Vaganov, and M. A. R. Munro, 2003: Summer temperature in northeastern Siberia since 1642 reconstructed from tracheid dimensions and cell numbers of *Larix cajanderi*. *Can. J. For. Res.*, **33**, 1905–1914, https://doi.org/10.1139/x03-109.

Peltier, D. M. P., and K. Ogle, 2019: Legacies of more frequent drought in ponderosa pine across the western United States. *Global Change Biol.*, **25**, 3803–3816, https://doi.org/10.1111/gcb.14720.

Peterson, T. C., and R. S. Vose, 1997: Global Historical Climatology Network - Monthly (GHCN-M), version 3. NOAA National Centers for Environmental Information, accessed 3 July 2022, https://doi.org/10.7289/V5X34VDR.

PRISM, 2023: Northwest Alliance for Computational Science and Engineering (NACSE). PRISM Climate Group Data Explorer, accessed 21 July 2022, https://www.prism.oregonstate.edu/explorer/.

Reid, E., and R. Wilson, 2020: Delta blue intensity vs. maximum density: A case study using *Pinus uncinata* in the Pyrenees. *Dendrochronologia*, **61**, 125706, https://doi.org/10.1016/j.dendro.2020.125706.

Saito, L., F. Biondi, J. D. Salas, A. K. Panorska, and T. J. Kozubowski, 2008: A watershed modeling approach to streamflow reconstruction from tree-ring records. *Environ. Res. Lett.*, **3**, 024006, https://doi.org/10.1088/1748-9326/3/2/024006.

——, ——, R. Devkota, J. Vittori, and J. D. Salas, 2015: A water balance approach for reconstructing streamflow using tree-ring proxy records. *J. Hydrol.*, **529**, 535–547, https://doi.org/10.1016/j.jhydrol.2014.11.022.

Salas, J. D., Z. Tarawneh, and F. Biondi, 2015: A hydrological record extension model for reconstructing streamflows from tree-ring chronologies. *Hydrol. Processes*, **29**, 544–556, https://doi.org/10.1002/hyp.10160.

——, J. A. Raynal, Z. S. Tarawneh, T. S. Lee, D. K. Frevert, and T. J. Fulp, 2016: Extending short records of hydrologic data. *Hydrology and Hydraulics*, V. P. Singh, Ed., Water Resources Publications, 717–760.

Seager, R., and Coauthors, 2007: Model projections of an imminent transition to a more arid climate in southwestern North America. *Science*, **316**, 1181–1184, https://doi.org/10.1126/science.1139601.

Shamir, E., D. Meko, R. Touchan, K. S. Lepley, R. Campbell, R. N. Kaliff, and K. P. Georgakakos, 2020: Snowpack- and soil water content-related hydrologic indices and their association with radial growth of conifers in the Sierra Nevada, California. *J. Geophys. Res. Biogeosci.*, **125**, e2019JG005331, https://doi.org/10.1029/2019JG005331.

Snee, R. D., 1977: Validation of regression models: Methods and examples. *Technometrics*, **19**, 415–428, https://doi.org/10.1080/00401706.1977.10489581.

Solander, K., L. Saito, and F. Biondi, 2010: Streamflow simulation using a water-balance model with annually-resolved inputs. *J. Hydrol.*, **387**, 46–53, https://doi.org/10.1016/j.jhydrol.2010.03.028.

St. George, S., and E. Nielsen, 2003: Palaeoflood records for the Red River, Manitoba, Canada, derived from anatomical tree-ring signatures. *Holocene*, **13**, 547–555, https://doi.org/10.1191/0959683603hl645rp.

Touchan, R., G. Funkhouser, M. K. Hughes, and N. Erkan, 2005: Standardized precipitation index reconstructed from Turkish tree-ring widths. *Climatic Change*, **72**, 339–353, https://doi.org/10.1007/s10584-005-5358-9.

Trumbore, S., P. Brando, and H. Hartmann, 2015: Forest health and global change. *Science*, **349**, 814–818, https://doi.org/10.1126/science.aac6759.

U.S. Census Bureau, 2024: Measuring America's people, places and economy. Accessed 5 January 2024, https://www.census.gov/.

Wahl, E. R., H. F. Diaz, J. E. Smerdon, and C. M. Ammann, 2014: Late winter temperature response to large tropical volcanic eruptions in temperate western North America: Relationship to ENSO phase. *Global Planet. Change*, **122**, 238–250, https://doi.org/10.1016/j.gloplacha.2014.08.005.

Wieder, W. R., D. Kennedy, F. Lehner, K. N. Musselman, K. B. Rodgers, N. Rosenbloom, I. R. Simpson, and R. Yamaguchi, 2022: Pervasive alterations to snow-dominated ecosystem functions under climate change. *Proc. Natl. Acad. Sci. USA*, **119**, e2202393119, https://doi.org/10.1073/pnas.2202393119.

Wigley, T. M. L., K. R. Briffa, and P. D. Jones, 1984: On the average value of correlated time series, with applications in dendroclimatology and hydrometeorology. *J. Climate Appl. Meteor.*, **23**, 201–213, https://doi.org/10.1175/1520-0450(1984)023<0201:OTAVOC>2.0.CO;2.

Wilks, D. S., 2019: *Statistical Methods in the Atmospheric Sciences*. 4th ed. Elsevier, 818 pp.

Williams, K. S., and D. G. Tarboton, 1999: The ABC's of snowmelt: A topographically factorized energy component snowmelt model. *Hydrol. Processes*, **13**, 1905–1920.

Winitsky, A. G., D. M. Meko, A. H. Taylor, and F. Biondi, 2023: Species sensitivity to hydrologic whiplash in the tree-ring record of the High Sierra Nevada. *Environments*, **10**, 12, https://doi.org/10.3390/environments10010012.

Wise, E. K., 2010: Tree ring record of streamflow and drought in the upper Snake River. *Water Resour. Res.*, **46**, W11529, https://doi.org/10.1029/2010WR009282.

Woodhouse, C. A., 2003: A 431-yr reconstruction of western Colorado snowpack from tree rings. *J. Climate*, **16**, 1551–1561, https://doi.org/10.1175/1520-0442(2003)016%3C1551:AYROWC%3E2.0.CO;2.

Yin, Z.-Y., X. Shao, N. Qin, and E. Liang, 2008: Reconstruction of a 1436-year soil moisture and vegetation water use history based on tree-ring widths from Qilian junipers in northeastern Qaidam Basin, northwestern China. *Int. J. Climatol.*, **28**, 37–53, https://doi.org/10.1002/joc.1515.

Yue, W., K. Seftigen, F. Chen, R. Wilson, H. Zhang, Y. Miao, Y. Chen, and X. Zhao, 2023: *Picea schrenkiana* tree ring blue intensity reveal recent glacier mass loss in High Mountain Asia is unprecedented within the last four centuries. *Global Planet. Change*, **228**, 104210, https://doi.org/10.1016/j.gloplacha.2023.104210.